Sensors & Actuators: B. Chemical 423 (2025) 136736

Contents lists available at ScienceDirect

Sensors and Actuators: B. Chemical

journal homepage: www.elsevier.com/locate/snb

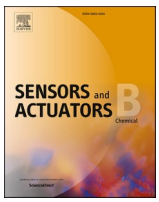

Neutrophil elastase specific fluorescent probe for early diagnosis of thyroiditis via serum sample testing and fluorescence imaging

Siqi Zhang [a], Mo Ma [a,c], Jingkang Li [a], Lanlan Xu [a], Pinyi Ma [a,*], Hui Han [b,*], Daqian Song [a,*]

[a] College of Chemistry, Jilin Province Research Center for Engineering and Technology of Spectral Analytical Instruments, Jilin University, Qianjin Street 2699, Changchun 130012, China
[b] Thyroid Surgery Department, General Surgery Center, First Hospital of Jilin University, Xinmin Street 1, Changchun 130012, China
[c] School of Pharmacy, Jilin University, Qianjin Street 2699, Changchun 130012, China

ARTICLE INFO

Keywords:
Neutrophil elastase
Low background fluorescence
Thyroid diseases
Fluorescence probe
Imaging *in vivo*

ABSTRACT

Autoimmune thyroid diseases (AITD) often interfere with early detection due to asymptomatic symptoms and normal thyroid function in routine tests. Developing early diagnostic tools is crucial for timely and accurate treatment, potentially reducing complications and improving patient outcomes. In this study, we developed Ox-NE, a novel fluorescent probe designed for the specific detection and quantification of neutrophil elastase (NE), a key biomarker of inflammation. Unlike the traditional probes, Ox-NE utilizes a unique mechanism that minimizes background fluorescence and enhances photostability, offering rapid, non-invasive, and apparent diagnostic capabilities. Ox-NE had a low limit of detection (LOD) of 1.54 μg/mL and exhibited high sensitivity and specificity with strong anti-interference properties. Through *in vitro* experiments, Ox-NE could accurately detect elevated NE levels in the serum of thyroiditis patients. Additionally, it could differentiate between normal thyroid cells, inflamed thyroid cells, and thyroid cancer cells. It also effectively facilitated the screening of sivelestat, a therapeutic agent for thyroiditis. Successful fluorescence imaging in mouse models further confirmed the potential of Ox-NE in advancing thyroid disease diagnostics.

1. Introduction

Autoimmune thyroid diseases (AITD), including Graves' disease (GD) and Hashimoto's thyroiditis (HT) [1,2], are organ-specific autoimmune disorders triggered by immune system dysfunctions [3–5]. These diseases often manifest subtly in their early stages, making detection through routine physical examinations challenging [6]. Patients may appear asymptomatic or have enlarged thyroid [7]. As the disease progresses, it can lead to hypothyroidism and other severe endocrine and metabolic complications [8,9], thereby increasing the risk of thyroid cancer [10]. Consequently, early diagnosis of these diseases is crucial for effective treatment and prognosis.

Despite their availability, diagnostic techniques such as serological tests, ultrasound imaging, and biopsies have limitations in terms of accuracy and convenience [11–16]. For instance, serological tests can detect specific antibodies but may lack sufficient sensitivity and specificity in certain cases [17,18]. Due to the invasive nature and technical constraints, ultrasound imaging and biopsies can cause unnecessary distress and pose risks to patients [19,20]. Fluorescence imaging, which is known for its rapidness, non-invasiveness, high sensitivity, high resolution, and low toxicity, offers a promising solution to these challenges [21–23]. The application of fluorescence probes, particularly in *in vitro* diagnostics and *in vivo* imaging, plays a critical role in diagnosing these diseases [24–29].

Neutrophil elastase (NE), which is a serine protease that is primarily expressed in neutrophils and can degrade various substances including elastin, collagen, and fibronectin, is involved in the progression of inflammation and bacterial infections [30,31]. The NE activity is approximately 80 % of the proteolytic activity in the human body, and the levels of fluctuations and activity can reflect the severity and status of diseases [32,33]. Building on preliminary studies that identified NE as a potential marker of inflammation, our research developed a novel fluorescent probe, Ox-NE, for serum sample testing and fluorescence imaging, aiming at diagnosing organ-specific inflammation and distinguishing between inflammation and cancer.

Previous studies on fluorescence probes for NE detection are primarily based on the internal charge transfer (ICT) principle. However, these molecules typically suffer from high background fluorescence,

* Corresponding authors.
E-mail addresses: mapinyi@jlu.edu.cn (P. Ma), hanhuijdyy@jlu.edu.cn (H. Han), songdq@jlu.edu.cn (D. Song).

https://doi.org/10.1016/j.snb.2024.136736
Received 8 July 2024; Received in revised form 19 September 2024; Accepted 2 October 2024
Available online 3 October 2024

insignificant spectral changes, and low sensitivity [34–39]. To address these issues, sodium dithionite ($Na_2S_2O_4$) was added into the reaction system to disrupt the conjugate structure of oxazine 1 and reduce background fluorescence. 4-Aminobenzyl alcohol allows for the appropriate separation between the enzyme recognition unit and the hydrophobic fluorescent group. The recognition unit was promoted to enter the internal cavity of the enzyme to improve the chemical stability of Ox-NE and the reactivity of NE. Furthermore, a pentafluoroalkyl group served as the recognition site of NE, covalently attached to 4-aminobenzyl alcohol. Upon interaction with NE, enzymatic catalysis cleaved the amide bond of the pentafluoroalkyl group. Ox-NE triggered the self-elimination of the linker, releasing CO_2 and forming oxazine 1, which emits strong red fluorescence. The spectral properties of Ox-NE were optimized, and its ability in specific recognition of NE and biocompatibility was thoroughly investigated. The results demonstrated that Ox-NE could successfully detect a significant increase of NE activity in the serum of patients with thyroid inflammation and provide precise quantitative analysis. Additionally, cell experiments and fluorescence imaging of an autoimmune thyroiditis mouse model further confirmed the potential of Ox-NE in diagnosing thyroid diseases. To our knowledge, this is the first study to explore a fluorescent probe that can specifically detect NE in thyroid organs, which lays a theoretical understanding of the association between NE and thyroid diseases.

2. Experimental procedure

2.1. Probe synthesis

The synthesis process of Ox-NE is displayed in Fig. 1.

2.1.1. Synthesis of compound 1

4-Aminobenzyl alcohol (1.00 g, 8.09 mmol) was dissolved in dichloromethane (CH_2Cl_2, 12 mL) in a round-bottom flask. And then 1 mL of triethylamine (TEA) was added in the round-bottom flask. After 2,2,3,3,3-pentafluoropropanoic anhydride (3.76 g, 12.14 mmol) was gradually added, the mixture was stirred at room temperature for 4 h. After completion of the reaction, the solvent was removed under reduced pressure through vacuum distillation. The crude product obtained was purified by silica gel chromatography using a mixture of dichloromethane and methanol (v/v, 8:1) as the eluent. The purification process yielded compound 1 as a light yellow solid, with a 24 % yield (100.96 mg). ^{1}H NMR (300 MHz, DMSO-d_6) δ 11.27 (s, 1H), 7.70 – 7.57 (m, 2H), 7.34 (d, J = 8.5 Hz, 2H), 5.22 (t, J = 5.7 Hz, 1H), 4.48 (d, J = 5.7 Hz, 2H) (Fig. S1). ^{13}C NMR (75 MHz, DMSO-d_6) δ 155.54, 140.75, 135.07, 132.07, 129.11, 127.40, 121.64, 62.85 (Fig. S2). HR-MS (m/z): Calculated for $[C_{10}H_7F_5NO_2]^-$: 268.0402, found: 268.0401 (Fig. S3).

2.1.2. Synthesis of compound 2

The synthesis procedure for compound 2 was adopted from the method described in the literature [40]. Initially, oxazine 1 (700 mg, 0.5 mmol) and sodium carbonate (Na_2CO_3, 212 mg, 2.0 mmol) were dissolved in 7.0 mL of water under a nitrogen atmosphere. Following this, 6 mL of CH_2Cl_2 was added. Sodium dithionite ($Na_2S_2O_4$, 409 mg, 2.0 mmol), dissolved in 10 mL of water, was then gradually introduced into the mixture. The reaction was stirred continuously at 40 °C for 1 h. Subsequently, TEA (100 μL, 0.7 mmol) was added dropwise under a nitrogen atmosphere and the reaction temperature was then reduced to below 0 °C. Bis(trichloromethyl) carbonate (100 mg, 0.3 mmol), dissolved in 5 mL of CH_2Cl_2, was slowly added to the reaction mixture. The mixture was stirred at 40 °C for an additional hour and then subjected to extraction with CH_2Cl_2. The organic layer was quickly separated and dried over anhydrous sodium sulfate (Na_2SO_4). The solvent was finally evaporated under reduced pressure at a temperature below 30 °C to yield compound 2 as a light green solid. The resulting crude intermediate was used immediately in the subsequent reaction without further purification.

2.1.3. Synthesis of Ox-NE

Under a nitrogen atmosphere, compound 2 (140 mg, 0.36 mmol) and compound 1 (100.96 mg, 0.375 mmol) were mixed and then pyridine (2 mL) and 4-dimethylaminopyridine (DMAP, 120 mg, 1.0 mmol) were added. The mixture was stirred at 45 °C for 1 h. After completion of the reaction, the solvent was removed under reduced pressure. The resultant residue was then purified by silica gel chromatography using petroleum ether and ethyl acetate (v/v, 2:1) as the eluent. This purification process yielded the fluorescent probe Ox-NE as a light blue solid (24 mg, 11 % yield). ^{1}H NMR (600 MHz, DMSO-d_6) δ 7.49 (d, J = 9.0 Hz, 2H), 7.35 (d, J = 7.7 Hz, 2H), 7.28 (d, J = 9.0 Hz, 2H), 6.39 (s, 2H), 6.32 (d, J = 11.6 Hz, 2H), 5.16 (d, J = 3.6 Hz, 2H), 3.33 (s, 8H), 1.07 (d, J = 7.1 Hz, 12H) (Fig. S4). ^{13}C NMR (151 MHz, DMSO-d_6) δ 155.68, 150.72, 146.02, 145.17, 143.99, 130.42, 129.53, 128.54, 125.13, 121.37, 119.44, 116.38, 106.85, 106.22, 100.14, 98.66, 69.59, 43.79, 12.32 (Fig. S5). HR-MS (m/z): Calculated for $[C_{31}H_{34}F_5N_4O_4]^+$: 621.2495, found: 621.2497 (Fig. S6).

2.2. Preparation of samples for spectrophotometric analysis

An Ox-NE stock solution (1 mM) was prepared in DMSO and stored at −80 °C in a light-protected environment to prevent degradation. Neutrophil elastase (NE) was dissolved in sterilized water to a concentration of 500 μg/mL and stored at −80 °C. For the experimental assays, the Ox-NE stock was further diluted in phosphate-buffered saline (PBS, pH 7.4, 10 mM) to a final concentration of 10 μM. The NE solution was added at varying volumes to obtain the desired concentrations, and the total volume of the mixture in each sample was maintained at 300 μL. A control sample without NE was also prepared for comparative analysis. Following the preparation of these standard solutions, serum samples obtained from the hospital, including those from normal individuals and thyroiditis patients, were processed using the same protocol. All samples were incubated at 37 °C on a shaker for 160 min to ensure thorough mixing and reaction completion before measurement. Spectrophotometric analysis was conducted using a 1-cm quartz cuvette at 37 °C.

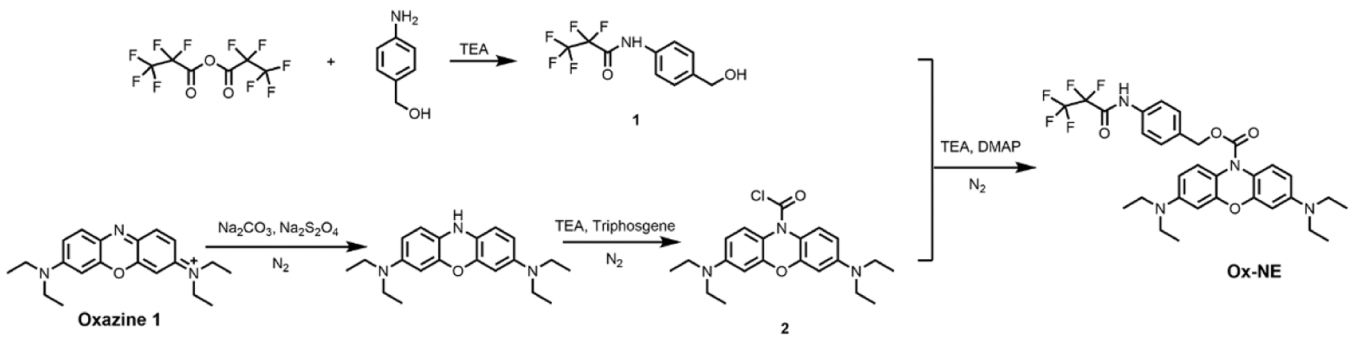

Fig. 1. The synthesis process of Ox-NE.

Fluorescence emission and UV-vis absorption spectra were recorded. The excitation and emission slit widths were set at 5 nm and 10 nm, respectively, the excitation wavelength was set to 635 nm, and the photomultiplier tube (PMT) voltage was set at 700 V.

2.3. Cell imaging procedures

In this experiment, two cell lines were utilized: normal thyroid cells (Nthy-ori3–1 cells, representative of normal thyroid epithelial cells) and TPC-1 cells (representative of thyroid cancer cells). Each of the cell lines was resuspended in fresh Dulbecco's Modified Eagle Medium (DMEM) supplemented with 10 % fetal bovine serum (FBS). The cells were then cultured in a controlled environment under 5 % CO_2 atmosphere at 37 °C. The cultivation continued until the cells reached confluence and formed a monolayer suitable for subsequent assays.

2.3.1. Imaging of cells incubated with Ox-NE for varying times

Nthy-ori3–1 cells were exposed to Ox-NE (10 μM) for different durations (10, 20, 40, and 60 min), and the optimal incubation time was determined.

2.3.2. Different means to induce endogenous inflammation in cells

Nthy-ori3–1 and TPC-1 cells were stimulated with lipopolysaccharide (LPS) for varying durations (24, 48, 72, and 96 h) or at different LPS concentrations (50, 100, and 200 μg/mL) to induce various levels of inflammation. After induction, Ox-NE (10 μM) was introduced, and the cells were incubated for 40 min prior to fluorescence imaging.

2.3.3. Medication screening for thyroiditis treatment

To assess the therapeutic efficacy of various treatments, Nthy-ori3–1 cells were first incubated with 100 μg/mL LPS for 96 h to simulate an inflammation condition. Subsequently, each of four different thyroiditis medications (menadione, ibuprofen, methimazole, and sivelestat) was administered to Nthy-ori3–1 cells, followed by an incubation period of 16 h. Then, Ox-NE (10 μM) was added to Nthy-ori3–1 cells, which were then subjected to fluorescence imaging.

2.4. Imaging of mice

This animal experiment was conducted in accordance with the ethical protocols established by the Institutional Animal Care and Use Committee (IACUC) of Jilin University, under the ethical inspection permit number SY202306031.

2.4.1. Establishment of an autoimmune thyroiditis mouse model

A water-in-oil emulsion was prepared by mixing porcine thyroglobulin (PTg) with complete Freund's adjuvant at a ratio of 1:1 to a final concentration of 0.25 mg/mL. This emulsion was administered subcutaneously at multiple sites under the dorsal skin of the mice at a total dosage of 50 μg per animal. The injections were carried out weekly for two weeks. From the third week, the emulsion was prepared from porcine thyroglobulin mixed with incomplete Freund's adjuvant at the same concentration and administered weekly for three additional weeks. The total dosage remained at 50 μg per animal and the injections were distributed among the dorsal, neck, and abdominal cavity regions. Additionally, the mice were provided with high iodine water (0.63 mg/mL).

2.4.2. Imaging of autoimmune thyroiditis mice

For fluorescence imaging, Ox-NE (80 μM, 200 μL) was injected near the neck region of the mice diagnosed with autoimmune thyroiditis. Imaging sessions were initiated two minutes post-injection while the mice were under anesthesia using isoflurane. A control group received Ox-NE injections in an identical manner. The imaging was performed using a small animal imager, and the dynamic changes in fluorescence signals were captured.

3. Results and discussion

3.1. Molecular design of Ox-NE

Although methylene blue (MB) is commonly used in fluorescence imaging, it suffers from low quantum yields and may generate toxic singlet oxygen upon excitation. Recent developments have introduced the oxazine 1 fluorescent group, which has been shown to more readily enter cells and exhibit brighter fluorescence in cellular environments [40]. To leverage these advantages, we selected the oxazine 1 fluorescent group due to its superior ability in cellular contexts. In our approach, $Na_2S_2O_4$ was added to the reaction system to reduce oxazine 1 and disrupt its rigid structure. The transformation from a rigid structure to a non-conjugated structure resulted in negligible UV-vis absorption and extremely low fluorescence, which are the highlights of the design of Ox-NE. Unlike most NE fluorescent probes that rely on the ICT mechanism, Ox-NE is based on the transition between conjugated and non-conjugated structures. This design theoretically leads to fluorescence quenching without the need for additional molecular mechanisms. 4-Aminobenzyl alcohol has been demonstrated to act as a self-cleaving linker that responds faster upon enzymatic triggering compared to other types of linkers. This flexible chain allows the molecule to fully penetrate the inner cavity of the enzyme and react with NE. Additionally, the pentafluoroalkyl group serves as the recognition site for NE. Ox-NE can quench fluorescence due to its non-conjugated structure, as well as its interactions with the recognition group to cleave the amide bond. The linker self-eliminates and forms the fluorescent group of oxazine 1, which exhibits strong fluorescence emission and near-infrared emission. Our functional modifications using the oxazine 1 fluorescent group resulted in low-background fluorescence, which is suitable for the specific detection of NE.

3.2. Spectral characterization before and after NE digestion

Initially, we explored the UV-vis absorption properties of Ox-NE, the reaction system, and the fluorescent oxazine 1 group. As depicted in Fig. 2A, Ox-NE exhibited a weak UV-vis absorption peak at 635 nm, which was then significantly enhanced upon the addition of NE to the reaction system. This is an indication of a more pronounced and superior UV-vis absorption peak at 635 nm of oxazine 1. This observation preliminarily confirms the fact that of oxazine 1 through the reaction of Ox-NE with NE. Furthermore, the color progression from lighter to darker among Ox-NE, the reaction system, and oxazine 1 depicted in Fig. 2A corroborates the conclusion that Ox-NE is cleaved and then the amount of oxazine 1 upon the addition of NE was increased, which leads to the gradual intensification of the blue color. Before exploring the fluorescence properties of Ox-NE, the optimal reaction time between Ox-NE and NE was determined by monitoring changes in fluorescence intensity every 20 min. As shown in Fig. S7, after the addition of 83 μg/mL of NE, the fluorescence intensity of the reaction system gradually increased, reaching a peak at 683.2 nm at 160 min, and then showed a steady trend after 160 min. Based on these findings, 160 min was selected as the optimal reaction time for Ox-NE with NE in the subsequent *in vitro* testing. Then, we explored the fluorescence spectral properties of the probe Ox-NE. As shown in Fig. 2B, under an excitation wavelength of 635 nm, Ox-NE exhibited a weak fluorescence emission peak at 683.2 nm, which was significantly enhanced upon the addition of 83 μg/mL of NE. The fluorescent group exhibited a more distinct and stronger fluorescence emission peak at 683.2 nm. This finding was consistent with the results of the UV-vis absorption spectra, further illustrating that NE cleaved Ox-NE to generate more oxazine 1. As the amount of NE was increased from 0 to 83 μg/mL, the fluorescence intensity of the reaction system at 683.2 nm gradually increased. The system showed a nearly 3.7-fold increase of the signal after the addition of 83 μg/mL of NE compared to that before NE addition (Fig. 2C). In Fig. 2D, we observed a linear correlation between the fluorescence

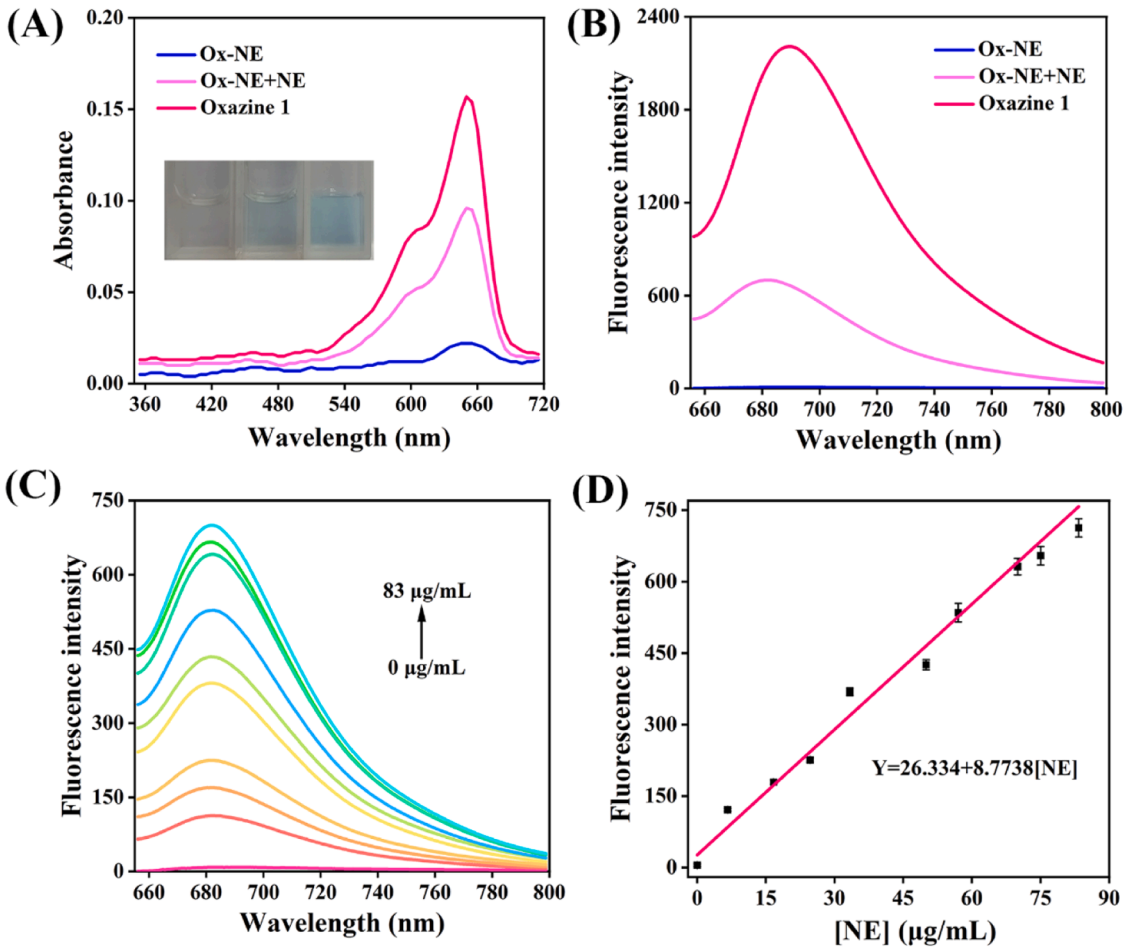

Fig. 2. (A) UV-Vis absorption spectra of Ox-NE (10 μM), the reaction system and oxazine 1 (10 μM). (B) Fluorescence spectra of Ox-NE (10 μM), the reaction system and oxazine 1 (10 μM); λ_{ex} = 635 nm. (C) Fluorescence spectra of Ox-NE following the gradual addition of NE; λ_{ex} = 635 nm. (D) Linear relationship between fluorescence intensity ($I_{683.2}$) of Ox-NE and NE concentration (0–83 μg/mL); λ_{ex} = 635 nm.

intensity of the reaction system and the concentration of NE. Subsequently, the low limit of detection (LOD) of Ox-NE was calculated to be 1.54 μg/mL using the 3σ/k formula. These results indicate that NE could effectively catalyze the transformation of Ox-NE into oxazine 1. In summary, the above results illustrate the potential of Ox-NE for precise quantitative measurement *in vitro*.

3.3. Condition optimization

We investigated the influence of different pH and temperatures on Ox-NE, the system, and oxazine 1, as well as their photostability, to assess the adaptability of Ox-NE to biological conditions. As shown in Fig. S8, the fluorescence intensity of both Ox-NE and the system remained relatively stable with minimal variation under both acidic and basic conditions. By contrast, the fluorescence intensity of oxazine 1 was enhanced under acidic conditions but remained stable at pH 7.4, which is the appropriate physiological pH. Consequently, pH 7.4 was selected as the optimal reaction pH (Fig. S8). Temperature optimization experiments demonstrated that the fluorescence intensity of Ox-NE and the system was somewhat invariant at 25 °C, 30 °C, 37 °C, and 42 °C, which is suggestive of their high stability across these temperatures. Although the fluorescence intensity of oxazine 1 was higher at 25 °C, it remained robust at 37 °C, which is the physiological temperature. Therefore, we selected 37 °C as the optimal reaction temperature (Fig. S9). Additionally, the photostability of Ox-NE and the system under light irradiation were investigated. As depicted in Fig. S10, the changes in fluorescence intensity of Ox-NE, the system, and oxazine 1 were negligible even after continuous light exposure for 1 h. This demonstrates the good photostability of Ox-NE. This result indicates that Ox-NE could resist decomposition under light irradiation, which is beneficial for applications such as *in vivo* imaging.

Overall, all the above results indicated that the optimal response conditions for Ox-NE were consistent with the physiological pH and temperature. Ox-NE possessed good resistance to light degradation. These findings suggest that Ox-NE is suitable for subsequent biological experiments.

3.4. Selectivity and inhibitor screening

We further investigated the specificity of Ox-NE towards NE by testing its responses against other commonly encountered biological substances, including cations, anions, amino acids, and various enzymes. 49 common biological substances were measured to confirm the selectivity of Ox-NE. The results, as depicted in Fig. S11, demonstrated that interference in Ox-NE by these substances was negligible compared to that in NE, confirming the high selectivity of Ox-NE for NE. Additionally, we introduced sivelestat, a specific inhibitor of NE, into the system. The presence of this inhibitor significantly reduced the fluorescence intensity of the reaction system, and this indicates that the enhanced fluorescence in the uninhibited reaction system was directly caused by the presence of the interaction between NE and Ox-NE. This outcome further substantiates the high specificity of Ox-NE for NE, as shown in Fig. S12. In conclusion, we confirmed the high specificity of Ox-NE for NE through selectivity and inhibitor screening assays. These

findings demonstrate that Ox-NE can respond to NE without being interfered with by other components in complex biological systems.

3.5. Molecular docking and response mechanism

Molecular docking experiments were conducted to simulate the interaction between Ox-NE and neutrophil elastase (NE). As illustrated in Fig. 3A, Ox-NE efficiently penetrated the active site of NE and engaged in a stable binding. This interaction allowed NE to cleave the recognition site on Ox-NE, resulting in the release of oxazine 1 and a consequent increase in fluorescence signal. The binding energy was calculated to be −8.3 kcal/mol, which is indicative of a strong interaction. Furthermore, Ox-NE formed three hydrogen bonds with His57, Ser195, and Val216 in NE, which is demonstrative of effective binding capabilities. The mechanism of sensing, as depicted in Fig. 3B, further corroborates these findings, showing how Ox-NE undergoes a structural transformation upon interacting with NE, leading to enhanced fluorescence. The mass spectrometry data in Fig. S13 also confirmed this conclusion. That is, Ox-NE and NE reacted to produce the fluorophore oxazine 1. Overall, these insights underscore the effectiveness of Ox-NE as a probe for NE, supporting its suitability for biological imaging applications and potential use in diagnostics and research.

3.6. Serum detection in thyroiditis patients

NE levels in serum have been identified as potential indicators of health and disease states. To investigate whether the expression of NE in serum correlates with thyroiditis, serum samples were obtained from both healthy individuals and thyroiditis patients. The fluorescence measurements of these serum samples were converted into specific concentrations using the previously established standard curve to allow for a comparative analysis of NE levels between healthy individuals and thyroiditis patients. As detailed in Table 1, the NE concentrations of serum from five normal samples were consistently low. In contrast, the NE concentrations of serum from patient samples were significantly higher. These results suggest that NE activity in the serum of thyroiditis patients may be higher than that of healthy individuals. Although the number of samples was low, the findings provided a promising direction for the development of blood-based biomarkers in the auxiliary diagnosis of thyroiditis. The results lay a foundation for future *in vitro* diagnostic tests for thyroiditis, indicating that there is a potential for using NE levels in serum as a diagnostic indicator for distinguishing between healthy individuals and thyroiditis patients.

Table 1
NE detection in serum for normal and thyroiditis patients using Ox-NE.

Patients status	Samples number	Found (μg/mL)	Average (μg/mL)	RSD (%)
Normal	1	0.86	0.95	8.63
		0.97		
		1.02		
	2	1.26	1.11	14.41
		1.13		
		0.95		
	3	2.24	2.03	8.87
		1.95		
		1.90		
	4	1.24	1.02	19.61
		0.87		
		0.94		
	5	1.94	1.78	7.87
		1.67		
		1.74		
Thyroiditis	1	3.18	2.79	20.43
		2.12		
		3.06		
	2	19.49	18.63	9.88
		16.51		
		19.88		
	3	9.07	9.34	13.92
		10.76		
		8.20		
	4	7.56	7.20	10.83
		6.30		
		7.73		
	5	6.68	6.82	19.35
		8.20		
		5.58		

3.7. Cytotoxicity assessment

A gradient of different concentrations of Ox-NE was added to Nthy-ori3–1 cells and the potential cytotoxic effects of Ox-NE on cellular health were evaluated. The CCK-8 assay was employed to measure cell

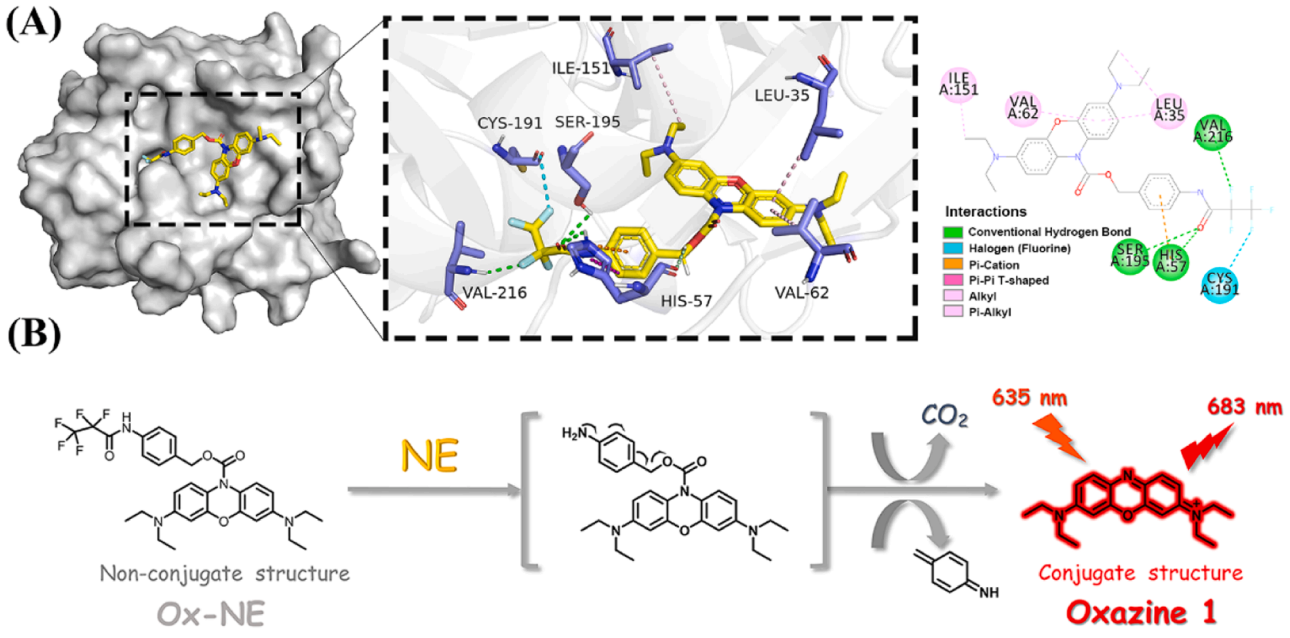

Fig. 3. (A) Simulation of interactions between Ox-NE and NE. (B) Mechanism of Ox-NE in sensing NE.

viability to ensure that Ox-NE does not inadvertently harm cells and their function during imaging. As depicted in Fig. S14, the results demonstrated that the viability of Nthy-ori3–1 cells remained high across all concentrations, consistently exceeding 90 % after incubating with various concentrations of Ox-NE for 24 h. This outcome unequivocally confirms the low cytotoxic of Ox-NE, indicating that even at high concentrations, the impact of Ox-NE on cells is minimal. The fact that Ox-NE had low cytotoxicity provides a solid foundation for subsequent cellular imaging and ensures that it is safe for application in biological contexts.

3.8. Imaging of cell incubating with Ox-NE for different incubation times

To determine the optimal incubation time for cell imaging using Ox-NE, we incubated Nthy-ori3–1 cells with a constant concentration of Ox-NE for varying durations and conducted fluorescence imaging. As illustrated in Fig. S15, the blank group (without Ox-NE) did not exhibit fluorescence. However, as the incubation time increased, the fluorescence intensity of Nthy-ori3–1 cells increased progressively over intervals of 10, 20, 40, and 60 min. The increase in fluorescence intensity indicates that Ox-NE interacts with endogenous NE, resulting in increased formation of fluorescent group oxazine 1. Taking into account several factors, including the fluorescence intensity of Nthy-ori3–1 cells, cell toxicity, and potential overexposure in subsequent inflammatory experiments, we proposed an incubation time of 40 min as the optimal time for probe incubation in future cellular imaging experiments. This time frame could balance effective imaging with minimal cellular disruption.

3.9. Different means to induce endogenous inflammation in cells

NE is recognized as a classical inflammatory marker for inflammation levels in targeted organs [30]. However, the correlation between NE expression in thyroid-targeted organ inflammation has not been reported. To explore this, we initiated the first investigation of NE in thyroid cells using lipopolysaccharide (LPS), a common inflammatory inducer derived from the outer wall of Gram-negative bacterial cells. Firstly, the incubation times of LPS with Nthy-ori3–1 cells were varied, and the changes in NE content were observed over time. Before imaging, the cells were incubated with LPS (100 μg/mL) for 24, 48, 72, and 96 h, followed by Ox-NE (10 μM) for 40 min. As shown in Fig. 4, Nthy-ori3–1 cells in the control group (Ox-NE only, no LPS) exhibited lower fluorescence due to the absence of inflammation. The fluorescence intensity of cells incubated with LPS for 48 and 72 h showed a slight increase. Surprisingly, the fluorescence intensity significantly increased at 96 h compared to earlier time points. This result suggests a significant increase of NE content in cells incubated with LPS for 96 h, and based on this marker, Ox-NE can easily differentiate between normal and inflamed thyroid cells.

As depicted in Fig. 4, regardless of the time periods, the fluorescence intensity of TPC-1 cells and their inflammation-induced counterparts were significantly lower compared to that of the corresponding Nthy-

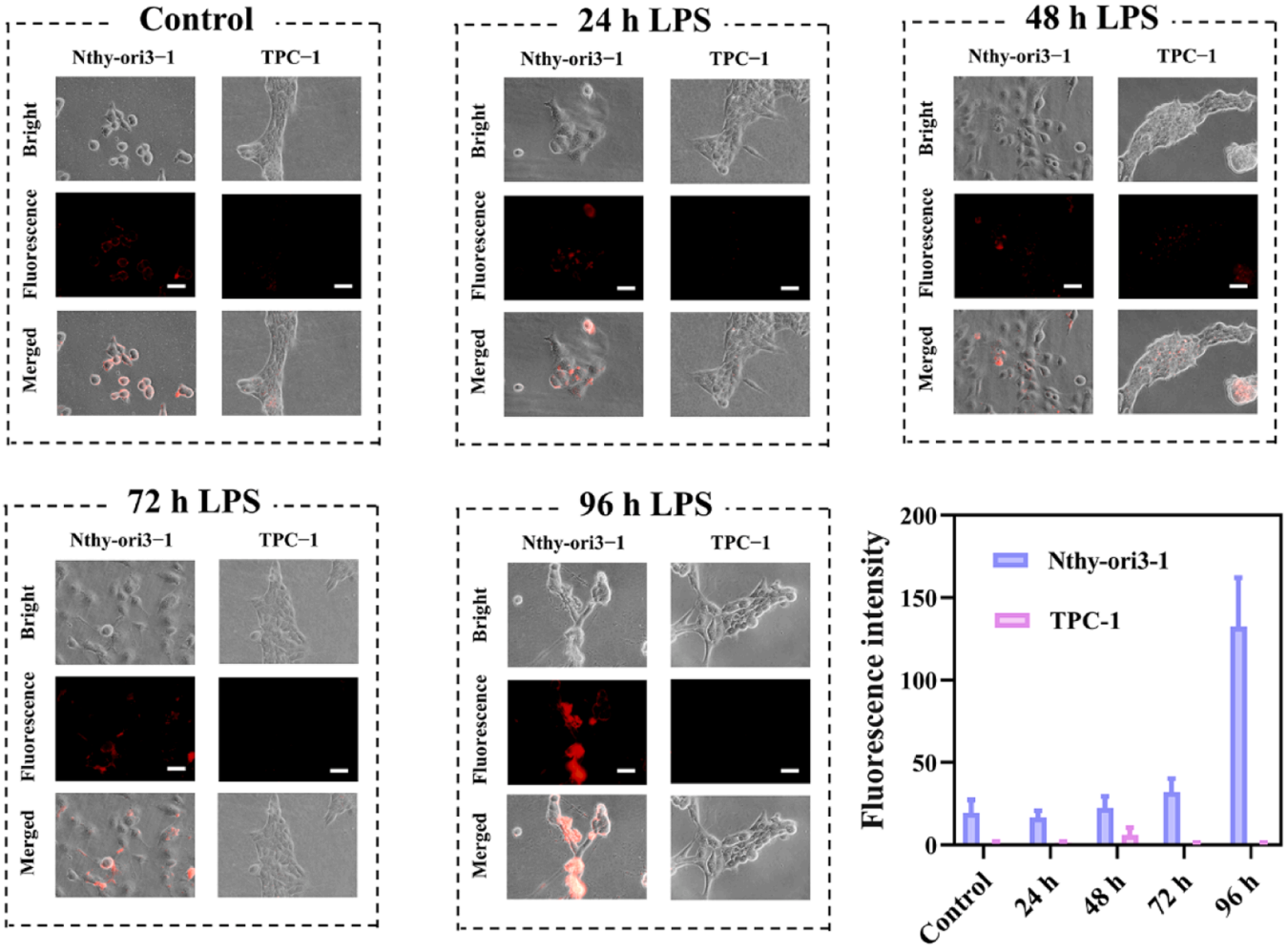

Fig. 4. Fluorescence imaging of Nthy-ori3–1 and TPC-1 cells after incubation with LPS for various times (24, 48, 72, and 96 h) followed by the addition of 10 μM Ox-NE, and comparison of fluorescence intensities obtained under these conditions. λex = 605–640 nm, λem = 670–715 nm. Scale bar = 50 μm.

ori3–1 cells at the same time points. This is likely due to the much lower NE content in TPC-1 cells, which allows minimal interactions between NE and Ox-NE, resulting in predominant non-conjugated probe structures and only a few oxazine 1 molecules, in turn, exhibiting weak fluorescence. During the induction of inflammation of cancer cells, NE levels remained nearly unchanged, showing lower levels. Based on these results, we inferred that both cancer and inflammation-induced cancer cells have significantly low NE levels and Ox-NE can easily distinguish between cancer and cancer-related conditions.

Building on prior experiments, we further explored the impact of different concentrations of LPS on inducing inflammation of Nthy-ori3–1 cells to understand how diverse LPS levels affect NE production. Based on the optimal incubation time of 96 h, we maintained this optimal incubation time while varying LPS concentrations to 50, 100, and 200 μg/mL. Following LPS treatment, cells were incubated with Ox-NE (10 μM) for 40 min before cellular imaging. As illustrated in Fig. S16, Nthy-ori3–1 cells in the control group displayed low fluorescence. However, the fluorescence intensity progressively increased with increasing LPS concentrations. A notable enhancement of cell brightness was observed at 100 μg/mL LPS, and the fluorescence intensity at 200 μg/mL LPS almost aligned with that at 100 μg/mL. This suggests a saturation point in NE production at 100 μg/mL. The fluorescence intensity histogram in Fig. S16 also revealed that, regardless of LPS concentration, the fluorescence intensity in TPC-1 cells and their inflammation-induced counterparts were consistently lower than that in Nthy-ori3–1 cells at the corresponding time points. During the inflammation induction in cancer cells, the fluorescence intensity was nearly zero, indicating extremely low NE levels. These findings align with previous results and further demonstrate that the probe Ox-NE can readily distinguish between cancer and cancer-related conditions. Notably, even in severe inflammatory conditions, TPC-1 cells exhibited significantly lower fluorescence intensity than Nthy-ori3–1 cells, which indicates that Ox-NE can also differentiate between inflamed cancerous tissues and normal tissues, thus has the potential to prevent misdiagnosis and treatment delays.

Collectively, the results from using these two methods to induce inflammation in cells demonstrate that Ox-NE can successfully differentiate between normal thyroid, thyroid inflammation, thyroid cancer, and cancer-related diseases. They also provide a critical theoretical foundation for the auxiliary detection and differentiation of complex diseases such as thyroid cancer-adjacent inflammation.

3.10. Medication screening for thyroiditis treatment

Recognizing the potential of enzyme inhibitors as effective treatments of thyroiditis, we conducted experiments to compare and screen the most effective NE-specific inhibitor, sivelestat, along with other commonly used thyroiditis medications. In this study, NE-specific inhibitors and three other thyroiditis medications were added to LPS-induced Nthy-ori3–1 cells. These medications were incubated with the cells for 16 h before adding Ox-NE (10 μM). The cells were then subjected to fluorescence imaging, and the fluorescence intensity was used as a critical marker for NE activity. As shown in Fig. S17, following the addition of sivelestat and three other medications, the fluorescence intensity decreased compared to the control group, which received only LPS without any medications. However, the reduction of fluorescence intensity was most significant in the group treated with NE-specific inhibitor, sivelestat, indicating that it has the strongest inhibitory effect on NE. This finding underscores the effectiveness of sivelestat as an NE inhibitor at the cellular level. It also indicates that with NE as a marker for thyroiditis, sivelestat can be observed through Ox-NE, and this can be the most effective treatment option. These insights could have far-reaching implications in treating thyroiditis, suggesting that targeting NE with specific inhibitors like sivelestat could significantly enhance treatment outcomes.

3.11. Imaging of autoimmune thyroiditis mice

The unique spectroscopic properties of Ox-NE and its exceptional potential for cellular differentiation have established it as a promising candidate for advanced biomedical imaging techniques. Building on this foundation, we successfully established an autoimmune thyroiditis mouse model to further validate and explore the capabilities of Ox-NE in *in vivo* applications. For the imaging experiments, Ox-NE (80 μM, 200 μL) was strategically injected near the neck area. This precise localization aimed to enhance the concentration of Ox-NE at the targeted site to maximize the fluorescence imaging efficacy. To monitor the changes in fluorescence signals at the thyroid sites of the mice, images were captured from 10 min to 40 min post-injection. As illustrated in Fig. 5, the mice in the experimental group exhibited significantly strong fluorescence at the thyroid site after Ox-NE administration. In contrast, the control mice, which did not have thyroid inflammation, exhibited only faint fluorescence. The robust response of Ox-NE within this brief time frame underscores its rapid detection capabilities, setting it apart from many other probes currently available. The pronounced difference in fluorescence intensity between the experimental and control groups highlights the high sensitivity and diagnostic potential of Ox-NE. This tool is a non-invasive method for detecting autoimmune thyroiditis *in vivo*. It not only can be utilized to enhance our understanding of thyroid disorders but also to facilitate the development of targeted therapeutic strategies.

4. Conclusions

In this study, a novel fluorescent probe, Ox-NE, was developed to specifically target and monitor the activity of NE in thyroiditis. The addition of $Na_2S_2O_4$ into the oxazine 1 disrupted its conjugated structure, which effectively reduced background fluorescence. The incorporation of 4-aminobenzyl alcohol as a self-cleaving linker allowed for deep penetration into the internal cavity of the enzyme, enhancing both chemical stability and enzymatic reactivity. The addition of a pentafluoroalkyl group, attached through a covalent bond to the self-cleaving linker, served as a specific recognition site for NE. The spectral properties of Ox-NE were optimized to evaluate its biocompatibility and confirm its specific NE-recognition capabilities. Ox-NE was successfully applied in the detection and quantification of the increased levels of NE in the serum of patients with thyroiditis. The cellular experiments demonstrated that Ox-NE could effectively distinguish between normal thyroid cells, inflamed thyroid cells with varying severities, and thyroid cancer cells. Furthermore, Ox-NE was proven effective in identifying

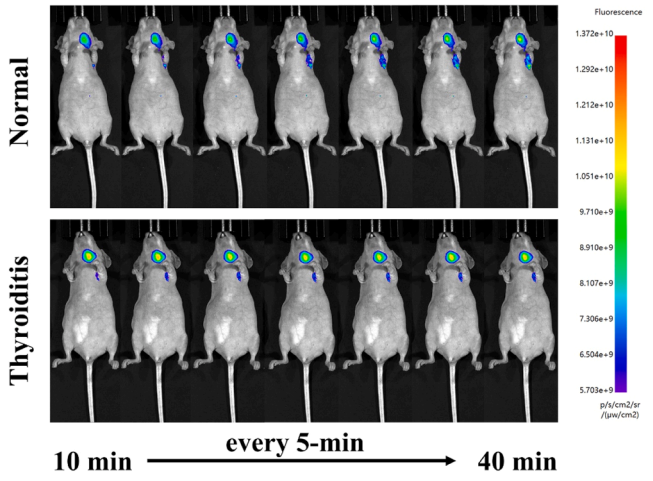

Fig. 5. Fluorescence images of normal mouse and autoimmune thyroiditis mouse injected with Ox-NE (80 μM, 200 μL) from 10 min to 40 min post-injection.

sivelestat as the optimal drug for targeting NE in thyroiditis treatments. Successful fluorescence imaging in an autoimmune thyroiditis mouse model underscored the potential of Ox-NE in detecting thyroid diseases, bolstering its applicability in the non-invasive monitoring of thyroiditis. These findings not only advance our understanding of thyroid-related conditions but also lay the groundwork for the future development of more precise and less invasive diagnostic techniques.

CRediT authorship contribution statement

Jingkang Li: Investigation, Data curation. **Lanlan Xu:** Investigation, Data curation. **Siqi Zhang:** Writing – original draft, Validation, Investigation, Data curation, Conceptualization. **Mo Ma:** Methodology, Investigation, Data curation. **Pinyi Ma:** Writing – review & editing, Software, Project administration, Data curation, Conceptualization. **Hui Han:** Project administration, Data curation, Conceptualization. **Daqian Song:** Supervision, Resources, Project administration, Funding acquisition.

Declaration of Competing Interest

The authors declare that they have no known competing financial interests or personal relationships that could have appeared to influence the work reported in this paper.

Data availability

Data will be made available on request.

Acknowledgement

This work was supported by the National Natural Science Foundation of China (22004046 and 22074052) and the Science and Technology Developing Foundation of Jilin Province of China (20230101033JC and 20210204130YY).

Appendix A. Supporting information

Supplementary data associated with this article can be found in the online version at doi:10.1016/j.snb.2024.136736.

References

[1] H. Fink, G. Hintze, Autoimmune thyroiditis (Hashimoto's Thyroiditis): current diagnostics and therapy, Med Klin. 105 (2010) 485–493.
[2] N. Daramjav, J. Takagi, H. Iwayama, K. Uchino, D. Inukai, K. Otake, et al., Autoimmune thyroiditis shifting from Hashimoto's thyroiditis to graves' disease, Medicina 59 (2023) 757.
[3] V.A. LiVolsi, The pathology of autoimmune thyroid disease: a review, Thyroid: Off. J. Am. Thyroid. Assoc. 4 (1994) 333–339.
[4] S. Synoracki, S. Ting, K.W. Schmid, Inflammatory diseases of the thyroid gland, Pathologe 37 (2016) 215–223.
[5] C.P. Schlicke, J.E. Hill, H.B. Arguinchona, Thyroiditis, Northwest Med. 64 (1965) 345–348.
[6] S.Y. Sheu, K.W. Schmid, Inflammatory diseases of the thyroid gland. Epidemiology, symptoms and morphology, Pathologe 24 (2003) 339–347.
[7] R.C. Mellors, W.J. Brzosko, L.S. Sonkin, Immunopathology of chronic nonspecific thyroiditis (autoimmune thyroiditis), Am. J. Pathol. 41 (1962) 425–437.
[8] Y. Luo, Y. Zhou, P. Peng, N. Yuan, X. Zhang, Prevalence and clinical correlates of suicide attempts in patients with first-episode drug-naïve major depressive disorder and comorbid autoimmune thyroiditis, Bjpsych Open 10 (2024) 1–7.
[9] D. Santoro, C. Vadala, R. Siligato, M. Buemi, S. Benvenga, Autoimmune thyroiditis and glomerulopathies, Front Endocrinol. 8 (2017) 119.
[10] I. Giagourta, C. Evangelopoulou, G. Papaioannou, G. Kassi, E. Zapanti, M. Prokopiou, et al., Autoimmune thyroiditis in benign and malignant thyroid nodules: 16-year results, Head. Neck-J. Sci. Spec. 36 (2014) 531–535.
[11] A. Ghaffari, R. Meurant, A. Ardakani, COVID-19 serological tests: how well do they actually perform? Diagnostics 10 (2020) 453.
[12] B. Dong, C.M. Galindo, E. Shin, C.J. Acosta, A.L. Page, M. Wang, et al., Optimizing typhoid fever case definitions by combining serological tests in a large population study in Hechi City, China, Epidemiol. Infect. 135 (2007) 1014–1020.
[13] M.W. Garry, J.F. Lopez, Comparison of the value of several serological tests in rheumatoid disease, Am. J. Med. Sci. 241 (1961) 225–230.
[14] R.M. Ferre, O. Chioncel, P.S. Pang, R.M. Lang, M. Gheorghiade, S.P. Collins, Acute heart failure: the role of focused emergency cardiopulmonary ultrasound in identification and early management, Eur. J. Heart Fail 17 (2015) 1223–1227.
[15] H. Zhang, Z. Meng, J. Ru, Y. Meng, K. Wang, Application and prospects of AI-based radiomics in ultrasound diagnosis, Vis. Comput. Ind. Biomed. Art. 6 (2023) 20.
[16] R.L. Sur, P.G. Borboroglu, J.L. Roberts, C.L. Amling, A prospective randomized comparison of extensive prostate biopsy to standard biopsy with assessment of diagnostic yield, biopsy pain and morbidity, Prostate Cancer P D. 7 (2004) 126–131.
[17] D.N.J. Lockwood, S. Sundar, Serological tests for visceral leishmaniasis - Have high sensitivity, but several limitations, Bmj-Br. Med. J. 333 (2006) 711–712.
[18] M.-A. Masella, H. Gallois, J.-C. Belisle-Pipon, Rapid serological tests and immunity policies: addressing ethical implications for healthcare providers and the healthcare system as a priority, Can. J. Bioeth. -Rev. Can. De. Bioethique 3 (2020) 177–179.
[19] Y.-J. Zhang, L. Wei, J. Li, Y.-Q. Zheng, X.-R. Li, Status quo and development trend of breast biopsy technology, Gland Surg. 2 (2013) 15–24.
[20] L. Zhuo, H. Wang, D. Chen, H. Lu, G. Zou, W. Li, Alternative renal biopsies: past and present, Int. Urol. Nephrol. 50 (2018) 475–479.
[21] E.E. Graves, R. Weissleder, V. Ntziachristos, Fluorescence molecular imaging of small animal tumor models, Curr. Mol. Med. 4 (2004) 419–430.
[22] J. Li, J. Cao, W. Wu, L. Xu, S. Zhang, P. Ma, et al., A molecular imaging tool for monitoring carboxylesterase 2 during early diagnosis of liver-related diseases, Sens. Actuators B-Chem. 377 (2023) 133122.
[23] L. Xu, H. Chu, D. Gao, Q. Wu, Y. Sun, Z. Wang, et al., Chemosensor with ultra-high fluorescence enhancement for assisting in diagnosis and resection of ovarian cancer, Anal. Chem. 95 (2023) 2949–2957.
[24] J. Chen, H. Jiao, W. Li, D. Liao, H. Zhou, C. Yu, Real-time fluorescence turn-on detection of alkaline phosphatase activity with a novel perylene probe, Chem. Asian J. 8 (2013) 276–281.
[25] H. Wen, X. Liu, S.-Q. Zhang, T. Yang, M.-L. Chen, J.-H. Wang, Discussion on definition of detection limit for ratio fluorescence pH sensing methods, Chin. J. Anal. Chem. 47 (2019) 597–604.
[26] M. Kamiya, Novel BIo-imaging Tools Based on the Precise Design of Functional Fluorescence Probes, Yakugaku Zasshi 136 (2016) 1355–1365.
[27] X.-L. Lu, W. He, Research advances in excited state intramolecular proton transfer fluorescent probes based on combined fluorescence mechanism, Chin. J. Anal. Chem. 49 (2021) 184–196.
[28] B.Y. Michel, D. Dziuba, R. Benhida, A.P. Demchenko, A. Burger, Probing of nucleic acid structures, dynamics, and interactions with environment-sensitive fluorescent labels, Front. Chem. 8 (2020) 112.
[29] Y. Tang, F. Pei, X. Lu, Q. Fan, W. Huang, Recent advances on activatable NIR-II fluorescence probes for biomedical imaging, Adv. Opt. Mater. 7 (2019) 215907.
[30] L. Winiarski, J. Oleksyszyn, M. Sienczyk, Human neutrophil elastase phosphonic inhibitors with improved potency of action, J. Med Chem. 55 (2012) 6541–6553.
[31] A. Sturrock, K.F. Franklin, S. Wu, J.R. Hoidal, Characterization and localization of the genes for mouse proteinase-3 and neutrophil elastase, Cytogenet. Cell. Genet. 83 (1998) 104–108.
[32] A. Belaaouaj, B.C. Walsh, N.A. Jenkins, N.G. Copeland, S.D. Shapiro, Characterization of the mouse neutrophil elastase gene and localization to chromosome 10, Mamm. Genome: Off. J. Int. Mamm. Genome Soc. 8 (1997) 5–8.
[33] B. Korkmaz, T. Moreau, F. Gauthier, Neutrophil elastase, proteinase 3 and cathepsin G: Physicochemical properties, activity and physiopathological functions, Biochimie 90 (2008) 227–242.
[34] X. Li, Y. Guo, Y. Qiu, X. Luo, G. Liu, Y. Han, et al., A novel strategy of designing neutrophil elastase fluorescent probe based on self-immolative group and its application in bioimaging, Anal. Chim. Acta 1237 (2023) 340617.
[35] X. Li, Y. zhao, Y. Qiu, X. Luo, G. Liu, Q. Sun, Phenoxazine-based red-emitting fluorescence probe for specific detection and imaging of endogenous neutrophil elastase in vitro and in vivo, Dyes Pigments 210 (2023) 110966.
[36] S.-Y. Liu, H. Xiong, R.-R. Li, W.-C. Yang, G.-F. Yang, Activity-based near-infrared fluorogenic probe for enabling in vitro and in vivo profiling of neutrophil elastase, Anal. Chem. 91 (2019) 3877–3884.
[37] T. Liu, X. Li, Y. Qiu, Y. Zhao, X. Luo, G. Liu, et al., A strategy for constructing novel red emitting fluorescent probes for neutrophil elastase tracking based on self-immolative linker and TICT effect, Dyes Pigments 222 (2024) 111872.
[38] Q. Sun, X. Li, Y. Guo, Y. Qiu, X. Luo, G. Liu, et al., Coumarin-based turn-on fluorescence probe with a large Stokes shift for detection of endogenous neutrophil elastase in live cells and zebrafish, Spectrochim. Acta Part A: Mol. Biomol. Spectrosc. 281 (2022) 121563.
[39] W. Zhang, Y. Zhou, D. Li, T. Ma, Near-infrared fluorescent probe with large stokes shift for detecting Human Neutrophil elastase in living cells, Spectrochim. Acta Part A: Mol. Biomol. Spectrosc. 252 (2021) 119533.
[40] J. Shang, X. Zhang, Z. He, S. Shen, D. Liu, W. Shi, et al., An oxazine-based fluorogenic probe with changeable pi-conjugation to eliminate false-positive interference of albumin and its application to sensing aminopeptidase N, Angew. Chem. Int Ed. Engl. 61 (2022) e202205043.

Siqi Zhang is currently a PhD student in College of Chemistry, Jilin University. Her interest is spectral analysis.

Mo Ma is currently a PhD student in College of Chemistry, Jilin University. His interest is spectral analysis.

Jingkang Li is currently a PhD student in College of Chemistry, Jilin University. His interest is spectral analysis.

Lanlan Xu is currently a PhD student in College of Chemistry, Jilin University. Her interest is spectral analysis.

Pinyi Ma gained his doctor's degree from College of Chemistry, Jilin University in 2017 and he is an associate professor in that school. His research areas are spectral analysis and biosensor.

Hui Han gained her PhD degree from College of Molecular Medicine, Laval University, Canada in 2018 and she is an associate senior doctor in 1st Hospital of Jilin University. Her research areas are enzyme of thyroid and breast disease.

Daqian Song gained his doctor's degree from College of Chemistry, Jilin University in 2003 and he is a professor in that school. His research areas are spectral and chromatography analysis.